

Wake dynamics of a fluttering, elongated bluff body

Zachary J. Taylor and Gregory A. Kopp

Boundary Layer Wind Tunnel Laboratory,
University of Western Ontario
London, Ontario, N6A 5B9, Canada
ztaylor@uwo.ca, gakopp@uwo.ca

Roi Gurka

Department of Chemical Engineering,
Ben Gurion University
Beer-Sheva, 84105, Israel
gurka@bgu.ac.il

ABSTRACT

Flow field measurements using streaming, time-resolved PIV for a rectangular cylinder undergoing flutter are reported. It is shown that the vortices shed from the body do not change their timing significantly compared to statically obtained Strouhal numbers providing evidence contradicting the current conceptual model. Through the phase averaged velocity field, kinetic energy and turbulent kinetic energy (TKE) are shown at points in the cycle where the flow loses the majority of its energy to the structure. The turbulent kinetic energy is observed to change relatively little between low and high amplitude motion revealing that turbulence may only play a second order effect in bluff body flutter. However, the TKE changes significantly within the cycle for the high amplitude case. The energy transfers within the wake, and with the body, are examined.

INTRODUCTION

The collapse of the Tacoma Narrows Bridge by bluff body flutter is one of the most well known engineering failures. In most introductory physics courses, it is taught that the failure is due to resonance associated with a von Kármán vortex street (Billah and Scanlan, 1991). However, it was not a Kármán vortex street which caused the collapse but a phenomenon experienced in airfoils as well: coupled flutter (Billah and Scanlan, 1991). This dangerous flow mechanism couples the torsional and vertical structural modes and, when there is insufficient mechanical damping, will result in greater and greater amplitudes of oscillation with increasing wind speed. Thus, as well as being a concern for the aviation industry, flutter is also a concern in the design of long span suspension bridges.

Long span suspension bridge cross-sections can be classified as elongated bluff bodies. An elongated bluff body is defined as one where the flow separates at the leading edge and reattaches along the body before subsequently separating at the trailing edge. Theodorsen's (1935) potential flow formulation of flutter is well suited for predicting onset of flutter for airfoils; however, it has proven inadequate for the prediction of flutter in elongated bluff bodies. The flow around such shapes, with large recirculating regions, is a stark departure from a potential flow. Thus, to prevent similar disasters as the Tacoma

Narrows Bridge collapse, all long span suspension bridges must be wind tunnel tested. Although the prediction of flutter by wind tunnel testing is well established, the understanding of the interaction between the flow and the structure is lacking. A model has been proposed for bluff body flutter involving the timing of leading edge vortices with the motion of the body. It is proposed that these vortices provide sufficient suction at the right phase of the model's motion to constantly amplify the motion with increasing wind speed. However, previous measurements by Taylor et al. (2007) show evidence to suggest that the timing of vortex shedding is relatively unaltered by the oscillations of the body. The fact that flutter is predicted for airfoils using potential flow (Theodorsen, 1935) also suggests that it is likely not governed through the timing of vortices.

The timing of leading edge vortices, however, has been observed to be necessary for the vortex shedding of static elongated bluff bodies. Nakamura and Nakashima (1986) observed that, for elongated bluff bodies with a splitter plate, vortices continue to be shed in an alternating pattern. They hypothesized that it was the leading edge shear layer's impingement that controlled the shedding of vortices from the leading edge which would convect into the wake and form the observed pattern. Naudascher and Wang (1993) noted that it was the impingement of vortices on the trailing edge that controlled the leading edge shear layer and referred to this instability as the impinging leading edge vortex (ILEV) instability. Later, Hourigan et al. (2001) found evidence that the trailing edge vortex shedding played an important role in the feedback which controls the leading edge vortex formation. Parker and Welsh (1983) performed experiments with a Reynolds number range of $1.48-3.11 \times 10^4$ and showed that there are four regimes with distinct vortex shedding characteristics for rectangular cylinders defined by their elongation – or chord/thickness – ratios. They found that for the regime $7.6 < c/t < 16$ there was no periodic vortex shedding detected and Mills et al. (2002) argue that the feedback required for the ILEV instability is suppressed at higher Reynolds numbers without external forcing. For the case of vortex-induced vibrations, Naudascher and Wang (1993) propose that the body motion, caused initially by the buffeting action of the wind, can provide the feedback necessary to re-excite the ILEV instability at higher Reynolds numbers.

However, flutter is a separate phenomenon to vortex-induced vibration. Vortex-induced vibration is a resonance between the structure and the oscillations of the vortex shedding wake. However, flutter does not occur at a harmonic of the shedding frequency. Thus, it is not expected that the ILEV instability should necessarily be excited due to the body motion during flutter.

Matsumoto et al. (1997), Takai and Sakamoto (2006) and Taylor et al. (2007) have all experimentally studied the case of rectangular cylinders in flutter. Takai and Sakamoto (2006) show the effects of damping as well as a change in elongation ratio on the onset of flutter. Matsumoto et al. (1997) observe that, rectangular cylinders with elongation ratios between 5 and 10, exhibit stability to flutter in a manner similar to the H-section of the Tacoma Narrows Bridge. Scanlan and Tomko (1971) show that for H-section models, the damping due to the aerodynamics quickly overcomes the structural damping of the mechanical system making flutter a negative damping phenomenon. Since both the structural and aerodynamic damping are non-conservative forces, if the summation of these is negative then the model absorbs more energy per cycle than is required and the amplitude must grow. Thus, it is evident that energy transfers of the structure and the flow are particularly important to the stability of elongated bluff bodies with increasing wind speed. Theodorsen's (1935) potential flow model and the work on flutter of airfoils leads to similarities with the phenomenon experienced for elongated bluff bodies; however, the flow around elongated bluff bodies is more turbulent and the kinetic energy balance is expected to be of importance for these types of bodies.

EXPERIMENTAL DETAILS

The experiments were performed in an open-return wind tunnel at the Boundary Layer Wind Tunnel Laboratory of the University of Western Ontario. The model was mounted to a rigid frame with four springs on either side allowing vertical and torsional motions. The model was freely mounted (i.e., not forced), thus, any motion is a direct result of the aerodynamic forces involved. The model had a chord-to-thickness ratio of 7 and a mass of 0.6 g/mm of span. The model was 19 mm thick with an aspect ratio (span/thickness) of 20. The torsional frequency of the spring-model assembly was measured to be 15.6 Hz with a damping ratio of 1.4% in still air. The Reynolds numbers tested are 18,500 and 22,500 based on model thickness.

Streaming, time-resolved PIV is used to measure the spatial details of the flow field, the temporal evolution of the flow field, as well as the position of the model. The position of the model was assessed based on the processing of the images taken by the PIV system. The air was seeded using olive oil yielding particle diameters on the order of 1 μm (Melling, 1997). The PIV system allows the capture of image pairs with a resolution of 1000 x 1000 pixels² at a rate of 500 Hz for up to 20 minutes using CMOS cameras and streaming to an optical disk array at a speed of 1.3 GB/s. The laser is a Nd:YLF laser with energy of 22 mJ/pulse when operating at 1000 Hz. In the current work, the data have been continuously sampled for 3 minutes at two different free stream speeds.

These two free stream speeds yield a case of "low" and "high" amplitude. In the comparison between the two experiments, the amplitude – instead of the free stream speed – will be the distinguishing term used herein. The image data yield 90,000 time resolved vector maps for each amplitude of motion. This number of samples allows convergence of turbulence parameters in each of the 16 phase bins of the sinusoidal motion. Phase averages were calculated based on 16 bins of the model's displacement, as determined from its location in the PIV images. The bins are each $1/16T$ seconds in length where T is the period of oscillation.

The image pairs of the PIV data were correlated using FFT cross-correlation with 32x32 pixels² interrogation windows and 50% overlap. Free stream particle image displacements were between 6-8 pixels. The data were both globally and locally filtered with less than 5% of vectors in each image being interpolated.

RESULTS

Motion of the model

The motion of the model during these experiments is steadily sinusoidal. At the velocities tested herein, the motion is controlled by the damping present in the system. However, when the free stream velocity was increased past that which was tested, the model oscillated so violently that it bounced off the top and bottom slots in the wind tunnel walls, which normally allow for free motion.

As mentioned above, there were two different free stream velocities tested yielding two different amplitudes of motion. The lower amplitude had a maximum angular displacement of just over 4° while the higher amplitude had an angular displacement of 10°. The frequency of the motion varied little throughout the measurements and the model vibrated at approximately 16 Hz. However, the motion of the model was not rotational about its central axis. Flutter of an airfoil is typically coupled flutter in which both the vertical and torsional modes are coupled by the fluid. Likewise, this was observed for the motion of the present experiments. The body was observed to rotate about a point one quarter of the chord from the leading edge. This is about the same location about which an airfoil rotates in coupled flutter and indicates that both the torsional and vertical modes were excited.

Flow structures in the wake

For the static case, Parker and Welsh (1983) found that for an elongation ratio of 7.6, a rectangular cylinder has intermittent and broad banded vortex shedding for Reynolds numbers similar to the present case. Taylor et al. (2007) found evidence that the wavelength of the shedding frequency and the intermittent nature of the vortex shedding do not change significantly during flutter. It appears that the timing of the wake from the static case is superposed on the wake through the angular travel of the body. However, Taylor et al. (2007) did not have phase averaged data to show the changes to typical turbulence parameters through the motion of the model. Presently, it is also found that the vortex shedding is intermittent. Figure 1 shows instantaneous contours of vorticity from which it is evident that significantly sized vortices are forming in the

wake when the body is close to its peak amplitude of 10° . From Figure 1 it is also shown that there is no arrangement of alternating vortices typical of a Kármán vortex street.

The cyclical nature of the motion allows for phase averaging based on the position and direction of the angular motion of the body. Thus, the 90,000 vector maps were binned into 16 phases and turbulence statistics were calculated for each bin and for each of the two amplitudes of motion. Figure 2 shows a vector map of the phase averaged velocity for the higher amplitude case in the same portion of the cycle as in Figure 1, near the peak amplitude of motion. In Figure 2, the vectors are viewed by an observer traveling at $0.75U_\infty$ which would reveal vortices if any were present in the phase average. The observation that no vortices are visible in the phase average implies that the frequency of the model and the frequency of the vortex shedding are unrelated.

Also of interest is the width of the wake. From Figure 2 it is observed that the width of the wake is on the order of the thickness of the body. The wake must be wider than for the static case because of the increased angle of attack; however, it is not observed to be substantially larger as might be expected from the motion of the model. Thus, the flux of momentum in the streamwise direction in each phase is not expected to change significantly from static even though the globally averaged wake will have a much greater momentum deficit than static. However, Figure 2 shows that the vertical momentum flux is non-zero and, thus, changed distinctly from static. It is noted that there is a slight curvature to the wake due to the lag between the fluid motion and the body motion. This curvature creates a circulation about the model. Circulation has a direct link with lift from thin airfoil theory; however, without data from around the body it is difficult to determine how far the circulation in the wake lags behind the circulation generated from the forces on the body.

Wake spectra

An advantage of using streaming time-resolved PIV is the ability to calculate both spatial and temporal spectra without the use of any assumptions. Taylor's hypothesis must always be invoked when generating spatial spectra from hot-wire measurements while conventional PIV systems do not have the temporal resolution to generate frequency spectra. Presently, both a frequency spectrum and wave number spectrum have been computed using time-resolved PIV data.

Of the available spatial spectra from PIV data, the $E_{11}(\kappa_1)$ spectrum was calculated. This spatial spectrum was calculated for selected rows in the x -direction in each PIV frame, and throughout the time series for the case of higher amplitude. These spectra were then averaged yielding a spatial spectrum consisting of 280,000 averaged spectra. The resulting wave number spectrum is then normalized similarly to Saddoughi and Veeravalli (1994) and shown in Figure 3(a). The cut off wave number of the spectrum is shown as a vertical dashed line and is estimated from the work of Foucaut et al. (2004) for PIV data obtained by cross-correlation, based on the size of the interrogation window. It is observed that the estimate of the Kolmogorov spectrum after the cutoff is highly noisy. A slope of $-5/3$ is plotted on the same figure, thus it is

concluded that the calculated spectrum is within the inertial sub-range and the data sampled herein do not have sufficient spatial resolution to resolve the dissipation range.

Frequency spectra were computed using the time series at a point in the wake. The PIV data were sampled at 500 Hz, thus, the spectrum is resolved up to 250 Hz in the frequency domain. For the higher amplitude case, the frequency spectrum of the vertical velocity at a point $5t$ from the end of the body into the wake and at $1.2t$ above the centerline of the wake is shown in Figure 3(b). Figure 3(b) depicts that most of the energy in the wake is centered about the frequency of the body's motion and its harmonics. However, of notable interest is the broad banded peak which occurs at the expected vortex shedding frequency. This frequency is expected based on the Strouhal number of symmetric rectangular cylinders that are both static and at zero angle of attack. The results of the frequency spectrum confirm that the vortex timing has not been significantly altered by the motion of the model. The spectra of the horizontal velocity shows that there is a discernable peak at the vortex shedding frequency but it is more pronounced in the spectra of the vertical velocity.

Since the flutter instability is not governed by a change in the vortex timing, a study of the kinetic energy in the wake is warranted. Flutter is the result of energy transfers between the flow and the body. Thus, since the timing of the body and the timing of the largest structures in the flow are not synchronized, it is of interest to determine the energy transferring mechanisms of the fluid.

Energy in the wake

The energy transfer is an important descriptor of turbulence. For flutter, energy balances are also of considerable importance for the stability of a given cross-section.

The total energy per unit mass at a point in a given fluid is the sum of the kinetic energy of the mean flow and the turbulent kinetic energy as follows,

$$\langle E(x, y) \rangle = 1/2 \langle u_i \rangle \langle u_i \rangle + 1/2 \langle u_i' u_i' \rangle \quad (1)$$

The angle brackets, in this case, refer to a phase average and the prime denotes a fluctuation from the phase average. The total energy in a control volume of a fluid per unit mass is the volume integral of (1). The PIV data analyzed here is in the wake, and as such, equating the energy absorbed by the model and that lost from the flow is not possible. However, by integrating vertical profiles of energy in the wake, it is possible to shed light on how energy is transferred to turbulence as well as to the body. Also, with the phase average, it is possible to understand at which points in the cycle the fluid has had greater energy exchanges with the body. An integral of the energy profiles (including the mean kinetic energy and the total energy) are shown in Figure 4 as they vary with phase angle, θ , through half of the cycle $0 < \theta < \pi$. It should be noted that, from (1), the difference between the two curves, for each level of oscillation amplitude, is the integral of the turbulent kinetic energy. The energy data in Figure 4 have been normalized by the square of the free stream velocity and the vertical direction is normalized by the thickness of the model. Thus, the comparison between the curves is relative to the total amount of energy initially available.

Therefore, the higher amplitude case has lost more energy to the model than the lower amplitude case not only absolutely, but also relative to the energy contained in the incoming stream of fluid.

The energy transfer between the model and the flow is the most important feature regarding the stability of flutter; in addition, the interchange of energy between the mean flow and the turbulent part of the flow is important. From Figure 4 it is evident that the level of turbulent kinetic energy in the flow changes through the motion. For the low amplitude case it is observed to be fairly consistent throughout the motion; yet, for the case of high amplitude motion the turbulent kinetic energy reaches a minimum value when the angular velocity of the model is a maximum.

The production of turbulent kinetic energy (TKE) is expressed as the coupling between the rate-of-strain and the Reynolds stresses,

$$P = -\frac{\partial \langle u_i \rangle}{\partial x_j} \langle u_i' u_j' \rangle \quad (2)$$

A positive value of P infers that energy is being transferred from the mean flow to the turbulent flow. Figure 5 shows a profile of turbulent kinetic energy production at $5t$ in the wake. The rate at which energy is being produced is thus significantly lower for higher amplitude in this same phase as lower amplitude motion. However, the TKE production is observed to vary throughout the body's motion more for higher amplitude than lower amplitude motion.

DISCUSSION

Unsteady aerodynamics is becoming increasingly important to better design such devices as miniature unmanned aerial vehicles. There are two broad classifications in unsteady aerodynamics: positive momentum flux and negative momentum flux flows. Positive momentum flux is for devices which provide thrust, such as a flapping airfoil (Bohl and Koochesfahani, 2009). Negative momentum flux applies to bodies which absorb energy from the flow – such as in the present case. These types of flows are occasionally implemented as power producing devices (Schmit et al., 2004); however, it is more typical that this type of phenomenon is crucial to avoid.

Scanlan and Tomko (1971) developed governing equations for bluff body flutter based on the model for potential flow by Theodorsen (1935). These are replicated here as the coupled dynamic system (3). The H_i^* and A_i^* coefficients are termed aerodynamic derivatives, for the aerodynamic derivatives they replace in Theodorsen's (1935) model. Angular motion is represented by α and vertical motion by h . A typical airfoil section, such as a NACA 0012 profile, has an A_2^* coefficient that is always negative with increasing wind speed (Scanlan and Tomko, 1971). Since this coefficient is proportional to the angular velocity of the model, it acts like a damping parameter. This aerodynamic damping term has significantly different characteristics for elongated bluff bodies which are unstable in flutter. For most shapes, the A_2^* coefficient begins negative for lower wind speeds; however, shortly before the onset of flutter this term begins approaching zero and goes positive.

$$\begin{aligned} m(\ddot{h} + 2\zeta_h \dot{h} + \omega_h^2 h) &= L \\ I(\ddot{\alpha} + 2\zeta_\alpha \dot{\alpha} + \omega_\alpha^2 \alpha) &= M \\ L &= \left(\frac{1}{2}\rho U_\infty^2\right)(2b) \left(kH_1^* \frac{\dot{h}}{U_\infty} + kH_2^* \frac{b\dot{\alpha}}{U_\infty} + k^2 H_3^* \alpha\right) \\ M &= \left(\frac{1}{2}\rho U_\infty^2\right)(2b^2) \left(kA_1^* \frac{\dot{h}}{U_\infty} + kA_2^* \frac{b\dot{\alpha}}{U_\infty} + k^2 A_3^* \alpha\right) \end{aligned} \quad (3)$$

Once this aerodynamic damping is positive and greater in magnitude than the structural damping, the system is dynamically unstable to increasing wind speed. The instability arises from the fact that the model extracts more energy from the flow per cycle than is required to sustain periodic oscillation. However, as noted, the current experiments were each for steady free stream speeds, low enough to allow for steady oscillation.

For a sprung dynamic system without the effect of damping there is a constant exchange between potential energy and kinetic energy and the system has steady oscillations at a given amplitude. For a system with non-zero damping, energy is extracted each cycle from the system and the amplitude slowly decays. Thus, since steady oscillations are observed, there must be a balance between the energy extracted by the structural damping of the system and the energy extracted from the fluid each cycle. The model proposed by Billah and Scanlan (1991) regarding vortex timing assumes that it is the leading edge vortices which contribute this energy to sustain the oscillations for the Tacoma Narrows Bridge. However, it was found herein that the timing of the vortex shedding and the timing of the oscillations are not synchronized. It was also found that the level of turbulent kinetic energy did not increase substantially between the case of low amplitude and that of high amplitude. Thus, the turbulence generated by the body does not appear to play a primary role in governing flutter. This observation may have been anticipated by the work of Theodorsen (1935), who predicted the onset of flutter with a potential flow model. However, the balance of energy throughout the cycle is of interest.

An important feature of Figure 4 is the portions of the cycle where the energy is a minimum. The energy has a local minimum at the phase of the cycle where the angular velocity of the model is at a minimum. The force due to damping is zero when the angular velocity of the model is zero. Thus, it appears that the model extracts most energy from the flow when the damping acts the least. This balance is analogous to the constant interchange of potential and kinetic energy for zero damping. However, there are now five main sources and/or sinks of energy in the system: potential and kinetic energy of the spring-mass system, mean and turbulent kinetic energy of the flow and structural damping.

It was shown in Figure 4 that for high amplitude the turbulent kinetic energy changes through the motion and reaches a maximum when the angular velocity of the model is a minimum. It has also been shown herein that turbulence is not the governing parameter in bluff body flutter based on the significant changes of the mean flow kinetic energy compared to the minor changes to the turbulent kinetic energy as well as the independence of timing between the turbulence and the model. The

interchange of the finite amount of energy between the model, the mean flow and turbulence reveals interesting features of the fluid-structure interaction. The model absorbs most of the energy at maximum angular amplitude, which is the same point when TKE approaches maximum levels. It might have been expected that since the flow was transferring the greatest amount of energy to the model at this phase that the mean flow would have less energy to produce turbulence. However, the opposite has been observed.

Some possible explanations behind these complex energy transfers is presented in the following paragraph. At the maximum amplitude of oscillation in the cycle, the potential energy should be maximum in the springs and the model is shown to receive more energy from the flow in this portion of the cycle. Some of this energy will be lost to damping and most of it will be converted into kinetic energy as the model obtains maximum velocity. However, some of the energy should go back into the fluid as the model – which can be thought of as a surface of the fluid – has considerable velocity at this phase of the cycle and is performing deformation work on the bounding surface of the fluid. Thus, it is possible that there is a phase lag factor to the production of turbulence through motion. This phase lag could occur in the following way. First, the flow has lost energy to the model while it moves slowly (Figure 4). When the model begins to accelerate it imparts some of the potential energy of the system back to the fluid through deformation of the fluid surface. Then, as the model slows down once again it loses the gained energy to turbulence and to the model. The TKE production shown in Figure 5 agrees with this description as the rate of energy transfer between the mean and the turbulent parts has slowed as the total energy of the fluid increases.

The level of TKE production requires further examination. TKE production remains relatively constant for the low amplitude case and varies significantly for the high amplitude case. The models both oscillate at the same frequency thus, for higher amplitude, the velocity gradient of the trailing edge must be higher than that of the lower amplitude motion. The shear typically driving the turbulence in the static case is aligned in the streamwise direction along the separated shear layers. However, since the trailing edge of the model has a high vertical velocity this motion provides a perpendicular direction of shear. Such a large scale motion may have an ‘organizing’ effect on the flow as well. It will have an effect on the rate-of-strain portion of (3); moreover, it is observed to decrease the Reynolds stresses (not shown) during this portion of the cycle. Thus, the large gradient imposed on the flow by the fast body motion seems to reduce the amount of energy transferred to turbulence until the motion slows.

CONCLUSIONS

Flutter is a negative damping phenomenon. Thus, energy transfer between the flow and the moving structure is of utmost importance. The measurements herein were made for steady sinusoidal motion, thus, the damping was sufficient in the system to control the motion.

It was found that the vortices being shed into the wake are not timed with the body motion, but the two time scales are independent. It was also observed that the turbulence –

in particular the turbulent kinetic energy – did not increase relative to the increasing body motion. These observations indicate that the turbulence plays a secondary role in the instability. Throughout the motion of the high amplitude case, complex energy transfers within the fluid were observed showing the effect of large structural motion interacting with the mean and turbulent flows.

REFERENCES

- Billah, K.Y., and Scanlan, R.H., 1991, “Resonance, Tacoma Narrows bridge failure, and undergraduate physics textbooks”, *Am. J. Phys.*, vol. 59, pp. 118-124.
- Bohl, D., and Koochesfahani, M., 2009, “MTV measurements of the vertical field in the wake of an airfoil oscillating at high reduced frequency”, *J. Fluid Mech.*, vol. 620, pp. 63-88.
- Foucaut, J., Carlier, J., and Stanislas, M., 2004, “PIV optimization for the study of turbulent flow using spectral analysis”, *Meas. Sci. Technol.*, vol. 15, pp. 1046-1058.
- Hourigan, K., Thompson, M.C. and Tan, B.T., 2001, “Self-sustained oscillations in flow around long blunt plates”, *J. Fluid Struct.*, vol. 15, pp. 387-398.
- Nakamura, Y., and Nakashima, M., 1986, “Vortex excitation of prisms with elongated rectangular, H and T cross-sections”, *J. Fluid Mech.*, vol. 163, pp. 149-169.
- Naudascher, E. and Wang, Y., 1993, “Flow-induced vibrations of prismatic bodies and grids of prisms”, *J. Fluids Struct.*, vol. 7, pp. 341-373.
- Matsumoto, M., Daito, Y., Yoshizumi, F., Ichikawa, Y. and Yabutani, T., 1997, “Torsional flutter of bluff bodies”, *J. Wind Ind. Aerodyn.*, vol. 69-71, pp. 871-882.
- Melling, A., 1997, “Tracer particles and seeding for particle image velocimetry”, *Meas. Sci. Technol.*, vol. 8, pp. 1406-1416.
- Mills, R., Sheridan, J. and Hourigan, K., 2002, “Response of base suction and vortex shedding from rectangular prisms to transverse forcing”, *J. Fluid Mech.*, vol. 461, pp. 25-49.
- Parker, R. and Welsh, M., 1983, “Effects of sound on flow separation from blunt plates”, *Int. J. Heat Fluid Flow*, vol. 4, pp. 113-127.
- Saddoughi, S. and Veeravalli, S., 1994, “Local isotropy in turbulent boundary layers at high Reynolds number”, *J. Fluid Mech.*, vol. 268, pp. 333-372.
- Scanlan, R., Tomko, J., 1971, “Airfoil and bridge deck flutter derivatives”, *J. Eng. Mech. Div. ASCE*, vol. 97, pp. 1717-1737.
- Schmit, R., Glauster, M., and Ahmadi, G., 2004, “Flow and turbulence conditions in the wake of a H-section in cross flow”, *J. Fluid Struct.*, vol. 19, pp. 193-207.
- Takai, K. and Sakamoto, H., 2006, “Response characteristics and suppression of torsional vibration of rectangular prisms with various width-to-depth ratios”, *Wind Struct.*, vol. 9, pp. 1-22.
- Taylor, Z.J., Gurka, R. and Kopp, G.A., 2007, “Wake measurements for a rectangular cylinder during torsional oscillation”, *7th Int. Symp. Particle Image Velocimetry, Rome, Italy*.
- Theodorsen, T., 1935, “General theory of aerodynamic instability and the mechanism of flutter”, *NACA Technical Note 496*.

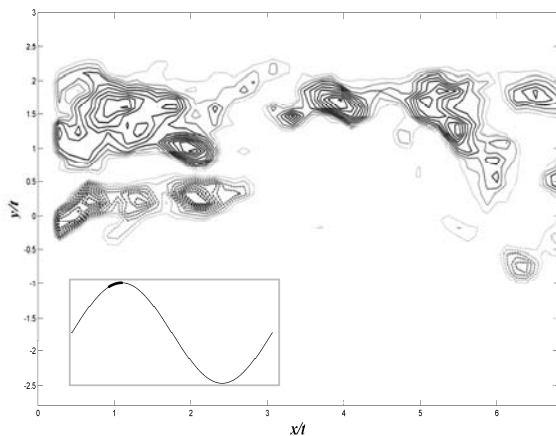


Figure 1 – Instantaneous vorticity contours of the case of higher amplitude. Inset curve shows the phase from which this instantaneous frame was taken (bolded portion of curve) where the curve represents the angular travel of the model.

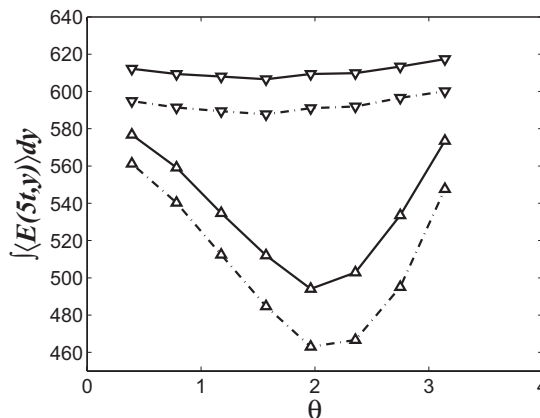


Figure 4 – Energy integrated over a vertical profile at $x=5t$ for the case of low amplitude (\blacktriangledown) and high amplitude (\blacktriangle) over the cycle. Dashed line is mean kinetic energy of the phase averaged flow and the solid line is the total kinetic energy of the phase.

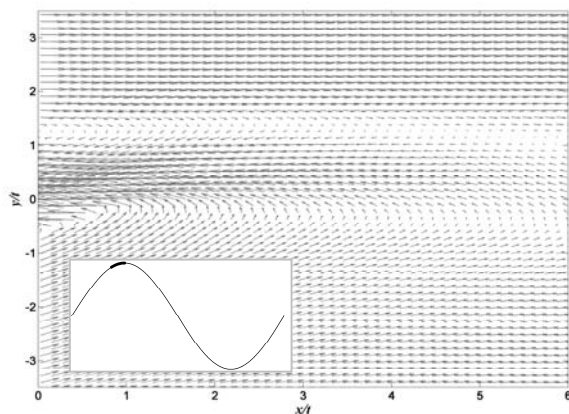


Figure 2 – Phase averaged vectors with 75% of the free stream speed subtracted from the horizontal component. Data is from the case of higher amplitude motion. Phase is as indicated by the inset.

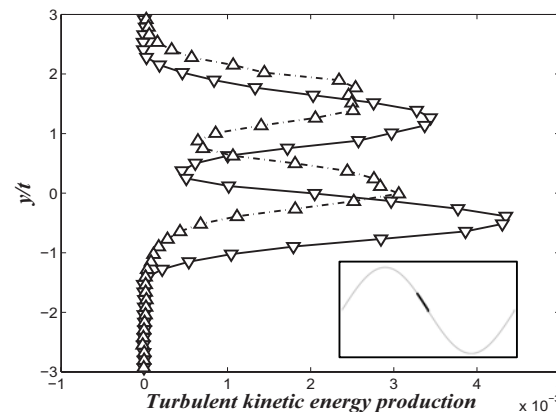


Figure 5 – Vertical profile of TKE production at $x=5t$ for the case of low amplitude (\blacktriangledown -solid) and high amplitude (\blacktriangle -dashed). Phase is as indicated by the inset.

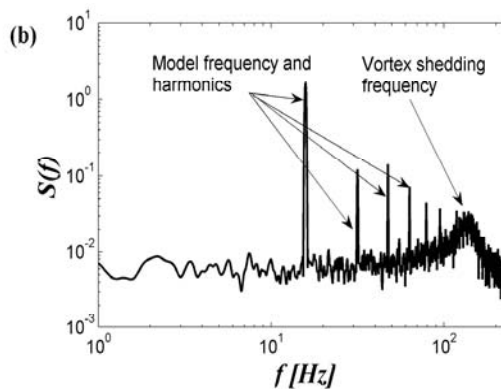
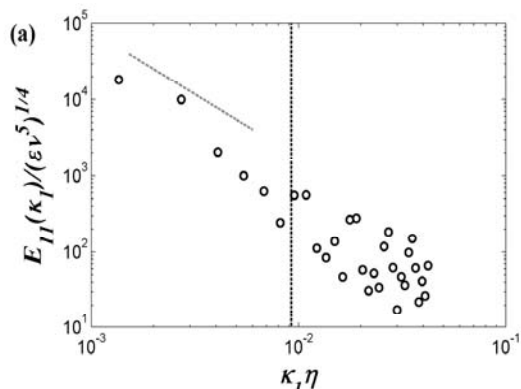


Figure 3 – From the case of high amplitude motion: (a) Wave number spectra, $E_{11}(\kappa_1)$, normalized based on Saddoughi and Veeravalli (1994). Vertical line marks the cutoff frequency based on the size of the PIV interrogation window and a $-5/3$ slope is indicated on the figure. (b) Frequency spectrum of vertical velocity at a point $(x,y)=(5t,1.2t)$.